 

PACS numbers: 42.55.Mv; 42.70.Df; 42.82.Et
DOI: 10.1070/QE2015v045n04ABEH015717

# Lasing in a nematic liquid crystal cell with an interdigitated electrode system

N.M. Shtykov, S.P. Palto, B.A. Umanskii, A.R. Geivandov

*Abstract.* **Waveguide lasing in a layer of a dye-doped nematic liquid crystal has been observed. The liquid-crystal layer was sandwiched between a quartz substrate and a glass cover plate on whose surface was deposited an interdigitated electrode system. This system had a period of 3.75 μm and played a dual role, namely, it created a spatial periodicity of the waveguide medium refractive index (thus creating distributed feedback) and served as a diffraction grating coupling out a part of waveguide radiation into the glass cover plate. The distributed feedback ensured lasing in the 18th diffraction order for the TE modes and in the 19th order for the TM modes of the waveguide. The generated radiation was observed at the exit from the glass plate end face at the angles to the waveguide plane of 33.1 ± 1.5° for TM modes and 21.8 ± 1.8° for TE modes. The intensity and position of the TE emission line showed no regular dependence on the voltage on the electrodes. In the case of TM radiation, an increase in the voltage led to a short-wavelength shift of the laser line and to a decrease in its intensity.**

***Keywords:*** *liquid crystals, dye lasers, planar dielectric waveguides, interdigitated electrodes.*

## 1. Introduction

The use of Bragg reflection of light from a periodic bulk inhomogeneity for the formation of distributed feedback (DFB) in lasers instead of the traditional Fabry–Perot scheme was proposed in work [1] together with a theory of coupled counterpropagating waves for periodic structures. The refractive index and gain in DFB lasers are periodically dependent on the coordinate. The DFB occurs when the Bragg condition is fulfilled, i.e., the inhomogeneity period $\Lambda$ is equal to an integer number of generated light half-waves, $\Lambda = m\lambda/(2n)$, where $m$ is the diffraction order (an integer number), $\lambda$ is the wavelength in vacuum, and $n$ is the refractive index of the material.

In laser schemes with diffraction gratings (DGs), coherent coupling between counterpropagating waves occurs only for waves satisfying the Bragg condition, because of which the amplification only of these waves leads to spectral selection of radiation. Although the DFB-based schemes most efficiently operate in the first diffraction order, in this case there exist problems of converging and collimating the strongly divergent beam emitted from the waveguide edge. Therefore, it seems more attractive to use the DFB scheme based on the second-order diffraction when radiation generated in the first diffraction order propagates normally to the waveguide plane with a low angular divergence. However, to develop schemes based on DFB in the first and second diffraction orders, it is necessary to create DGs with very short periods.

Despite a lower DFB efficiency, DGs with a large period are advantageous due to the possibility of their production using the well-developed methods of photolithography and ion-plasma etching. In [2], feedback was achieved using the 12th diffraction order. The DG had the period $\Lambda \approx 2$ μm and was placed inside the emitter of an InGaAs laser operating at the wavelength $\lambda = 1.06$ μm. The use of similar gratings with large periods and DFB in the 6th and 25th diffraction orders was demonstrated in studies [3, 4].

Waveguide lasers with DGs and emission through the substrate [5] are of interest as sources of radiation with a narrow directional pattern [6]. Lasers emitting through the grating can be divided into two types, with distributed reflectors [6, 7] and with DFB [5, 8]. In the latter case, one can use quarter-wave shifted DGs in order to improve the directional pattern.

In recent years, laser effects in liquid crystals (LCs) doped with dyes have been extensively studied. Interest in these effects is stimulated by the possibility of creating compact tunable organic lasers with DFB and a low lasing threshold, which are highly sensitive to a variety of external factors, such as light, pressure, electric and magnetic fields, chemical additives, and so on. Most studies are devoted to lasing in dye-doped cholesteric LCs, which have a periodic (spiral) internal structure [9–13]. Unfortunately, principal topological limitations do not allow one to smoothly change the cholesteric spiral pitch and, hence, the laser wavelength using electric or magnetic fields [14]. Probably, the periodic structures based on nematic liquid crystals (NLCs) are more suitable for smooth tuning of the intensity and spectral position of laser lines.

An LC cell consisting of two glass plates was used in [15]. The surface of one of the plates was coated by a transparent conducting ITO layer, while a nontransparent chromium interdigitated electrode system (IES) with a period $\Lambda \approx 15$ μm was formed on the surface of other plate. This system played a dual role. First, it served as a shadow mask creating a spatially periodic gain distribution in the pumped region of the cell. Owing to this, lasing was observed even in the isotropic phase of an NLC in the 71–79th diffraction orders. Second, in the nematic phase, when an electric field was applied between the transparent electrode on one glass and the nontransparent electrodes of the IES on the other glass, a spa-

**N.M. Shtykov, S.P. Palto, B.A. Umanskii, A.R. Geivandov**
A.V. Shubnikov Institute of Crystallography, Russian Academy of Sciences, Leninsky prosp. 59, 119333 Moscow, Russia;
e-mail: nshtykov@mail.ru
Received 14 November 2014
Kvantovaya Elektronika **45** (4) 305–311 (2015)
Translated by M.N. Basieva

tially periodic modulation of the refractive index was formed due to reorientation of the NLC director above the nontransparent electrodes of the system. Using this configuration of the NLC cell, the authors of [15] observed an electric field-induced shift of the laser spectrum by 25 nm in the region of the dye fluorescence.

In the present work, we study waveguide lasing in a cell whose configuration is similar to that described in [15]. The main attention is paid to the parameters of laser radiation emitted from the NLC waveguide into the glass cover plate as a result of diffraction on the IES.

## 2. Experimental scheme and results

The scheme of the cell used in our experiments is shown in Fig. 1. The IES ($\Lambda$ = 3.75 μm, chromium electrode width 1.75 μm, interelectrode gap width $l$ = 2 μm) was formed on a glass plate and contacted the NLC layer. The second plate, which, together with the first one, formed a plane capillary filled with the LC, was made of fused quartz with bevelled polished end faces. The NLC layer thickness (capillary thickness) was controlled by spacers (Teflon film strips of calibrated thickness) and measured interferometrically from the light transmission spectra for the cell without an LC. We used two cells with thicknesses of 13.8 ± 0.2 and 3.2 ± 0.3 μm. To achieve a homeotropic orientation of the NLC layer director (the optical axis is directed normally to the layer plane), the surfaces of both plates were coated by a thin film of chromolan (chromium stearyl chloride).

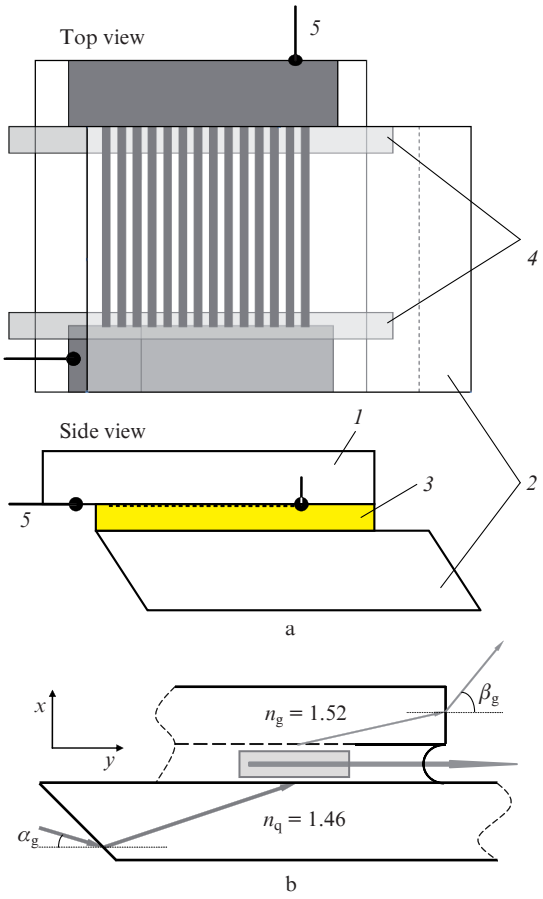


**Figure 1.** (a) Scheme of the cell [(*1*) glass plate with an IES on the inner surface contacting the NLC layer; (*2*) fused quartz plate with polished faces bevelled at an angle of 45° with respect to the working planes; (*3*) dye-doped NLC layer between the plates; (*4*) Teflon spacers; (*5*) wires connecting the IES with a voltage supply] and (b) scheme of propagation of pump and fluorescence beams in the NLC cell.

A sinusoidal voltage, which was applied to the IES, formed in the NLC layer a spatially periodic (along the $z$ axis) electric field (Fig. 1), which caused periodic variations in the effective (extraordinary) refractive index of the NLC. The voltage frequency was chosen to be 5 kHz to avoid hydrodynamic instability observed in NLCs at low frequencies. The gap between the waveguide claddings was filled with the solution of dye in the NLC due to capillary forces. We used an LZhK-2 NLC mixture specially developed in our laboratory for these experiments, which was doped with DCM dye [4-(Dicyanomethylene)-2-methyl-6-(4-dimethyl-amino-styryl)-4*H*-pyran] with a weight concentration of 0.6%. In the experiment, the $xz$ plane is horizontal and the direction of rotation of the spectrometer detector is oriented along the $y$ axis, i.e., vertically. The cells were optically pumped by a semiconductor laser (wavelength 445 nm, cw power 320 mW) or by the third harmonic (355 nm) of a pulsed neodymium laser.

A pump beam linearly polarised in the $xz$ plane entered the quartz plate through the front face bevelled at the angle $\alpha_g$ to the waveguide plane (NLC layer), was refracted at the interface and fell on the NLC layer at a small grazing angle. As a result, the pumped region had a strongly elongated shape with the major axis directed along the $z$ axis, i.e., parallel to the wave vector of the diffraction grating (IES). The fluorescence radiation propagates in the NLC layer as in a planar waveguide and leaves it through the end face meniscus. A part of this radiation diffracted on the IES is refracted into the glass plate and the other part is reflected to the NLC layer. The radiation leaves the glass plate through its end face at an observation angle $\beta_g$.

The end face of the glass plate, which was obtained by cutting the IES from a large piece, is not a perfectly polished surface with a single plane of refraction. The refraction planes of different regions of this surface deviate from the average value by several degrees. Therefore, the angles of observation of lasing peaks from different (with respect to the grating height) pumped regions of the IES also differed by several degrees. The observation angles averaged over multiple measurements were $\beta_g$ = 33.1 ± 1.5° for TM modes and $\beta_g$ = 21.8 ± 1.8° for TE modes.

When pumping the cell by radiation of a semiconductor laser (445 nm) having an intensity of 6.3 kW cm$^{-2}$, we observed fluorescence in a wide range of angles (Fig. 2); the fluorescence was weakly polarised and demonstrated no angular dependences. The pump pulse repetition rate was 10 Hz, the pulse duration was 20 μs, and the pumped region size was 15 × 343 μm.

A different fluorescence pattern is observed upon pumping by the third harmonic of a neodymium laser (355 nm, pulse duration 11 ns). In this case, the pump intensity (1.6 MW cm$^{-2}$) is considerably higher, the size of the pumped region is 75 × 1200 μm, and the fluorescence spectrum has two peaks (Fig. 2). The beam emitted at the angle $\beta_g$ = 34° is polarised horizontally (in the $xz$ plane, which corresponds to the polarisation of TM waveguide modes), while the radiation emitted at the angle $\beta_g$ = 23° is polarised vertically (along the $y$ axis, which corresponds to the polarisation of TE modes). With the use of a narrow slit aperture, we found that radiation at these observation angles is emitted from the end face of glass with the IES.

As one can see from the dependences presented in Fig. 2, the intensity of radiation from the waveguide end face ($\beta_g$ = 0) is considerably lower than of radiation from the cover glass. This is probably related to the fact that the end face meniscus of the NLC waveguide plays the role of a very short-focus lens, which leads to a significant angular divergence of radiation. In this case, the spectrometer detector with the input aperture ~6 mm in diameter receives only a small part of radiation emitted from the waveguide.

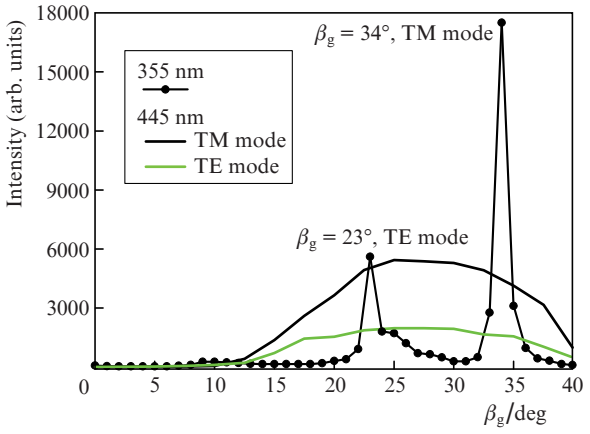


**Figure 2.** Dependences of the radiation intensity in the fluorescence maximum of a mixture of 0.6% of DCM with LZhK-2 on the recording angle upon pumping by the third harmonic of a neodymium laser (curve with dots) and by a semiconductor laser (solid curves, fourfold scale). The cell thickness is 13.8 ± 0.2 μm.

The emission spectra in the case of pumping by a semiconductor laser (Fig. 3a) have a shape and a width at half maximum typical for fluorescence spectra of dyes, which points to the absence of amplification in the medium. When the cell is pumped by the third harmonic of a neodymium laser (Fig. 3b) with a high intensity (1.6 MW cm$^{-2}$), the emission spectra become considerably narrower, which testifies to the occurrence of some amplification. The fine structure of the spectra points to multimode radiation. Indeed, estimates show that, at the waveguide thickness of 13.8 μm, the dye fluorescence spectrum can contain approximately 25 TM and 25 TE modes, and some of them can satisfy the lasing conditions.

To decrease the number of modes in the fluorescence spectrum, we made a 3.2-μm-thick cell. The inset in Fig. 4a shows the dependence of the fluorescence (lasing) intensity on the pump pulse energy. Pumping was performed by the third harmonic of a neodymium laser into a region with dimensions 75 × 800 μm. Assuming that the threshold pump pulse energy is 9.5 μJ, the threshold intensity for the given pumped region size and pulse duration should be 1.58 MW cm$^{-2}$. In [15], the lasing threshold for the DCM dye was 0.18 MW cm$^{-2}$. However, it was measured in the isotropic NLC phase upon pumping by the second harmonic (532 nm) of a neodymium laser, which coincided with the absorption maximum of the dye.

The laser spectra above the threshold are presented in Fig. 4. As can be seen from comparison of the radiation spectra presented in Figs 3 and 4, the laser lines are noticeably (by ~30 nm) shifted to long wavelengths with respect to the dye fluorescence maximum (Fig. 3a). The results described above were obtained in the absence of electric voltage on the IES.

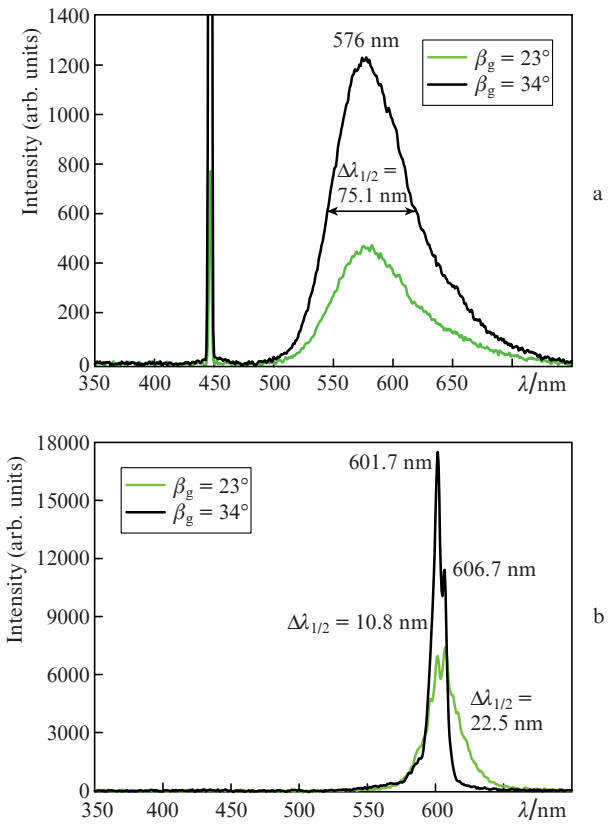


**Figure 3.** (a) Luminescence spectra observed at the angles $\beta_g$ = 23° (TE mode) and 34° (TM mode) upon pumping by a semiconductor laser with an intensity of 6.3 kW cm$^{-2}$ and (b) superluminescence (lasing) spectra observed at the same angles upon pumping by the third harmonic (355 nm) of a neodymium laser. The cell thickness is 13.8 ± 0.2 μm.

As to the dependence of the fluorescence (lasing) intensity on the value of the voltage applied to the IES, for TE modes we observed no regular correlation of this intensity with the voltage varying within the range 0–15 V. On average, the intensity does not change and the radiation polarisation is retained. In the case of TM modes, the radiation intensity at low voltages slightly increases (Fig. 5), but even at voltages above 1.2 V it monotonically decreases in amplitude, while the laser line broadens and shifts to short wavelengths. The radiation polarisation does not change. In our case, the shift of radiation spectra caused by the electric field is about 8 nm, which is almost fourfold smaller than the shift observed in [15]. This is obviously related to a different geometry of the field applied to the NLC layer and, hence, to a different topology of deformation of the NLC director (i.e., its optical axis).

## 3. Interpretation of experimental results

### 3.1. NLC waveguide modes

Let us ignore the existence of the IES on one of the interfaces of the NLC waveguide and calculate its mode composition under the conditions corresponding to the experiment. In our case, the LC layer with the thickness $d$ = 3.2 μm (Fig. 6) was sandwiched between a quartz plate with the refractive index $n_q$ = 1.46 and a glass plate with the refractive index $n_g$ = 1.519. The LC in the waveguide was oriented homeotropically, i.e., its director and optical axis were oriented along the $x$ axis. The refractive indices of the LZhK-2 LC in the directions per-

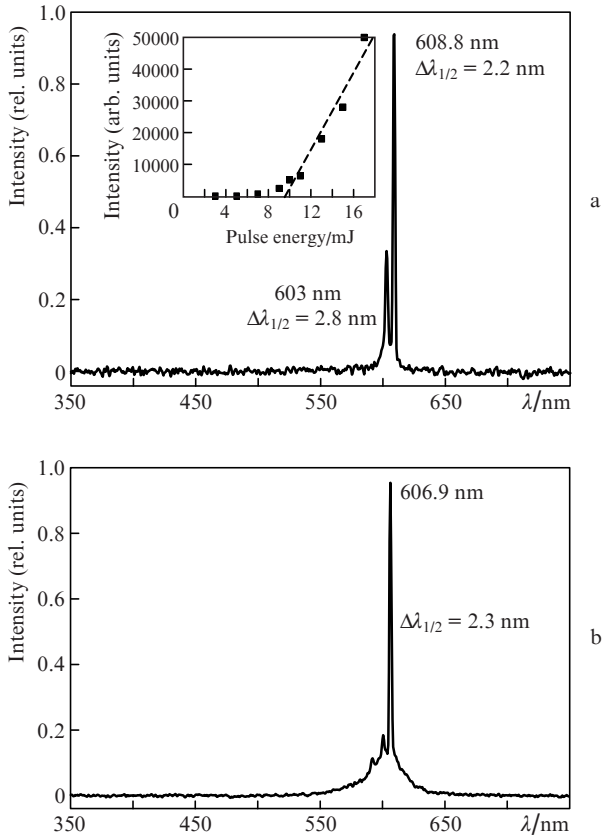


**Figure 4.** (a) TM mode oscillation spectrum at $\beta_g = 32.5°$ and a pump intensity of 2.2 MW cm$^{-2}$ (the inset shows the dependence of the fluorescence (lasing) intensity on the pump pulse energy), as well as (b) TE mode oscillation spectrum at $\beta_g = 23°$ and a pump intensity of 2.75 MW cm$^{-2}$.

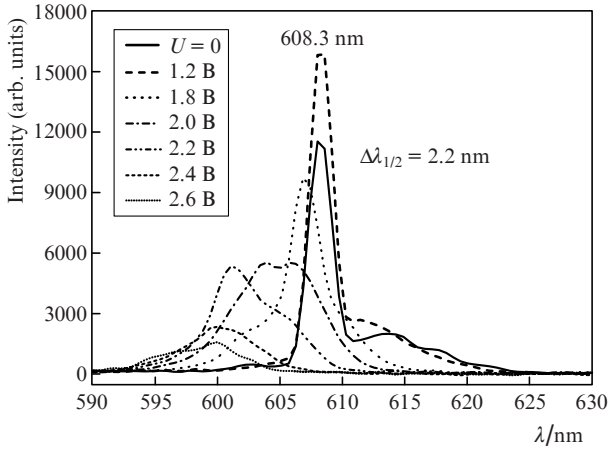


**Figure 5.** Dependence of TM-mode oscillation spectra on the sinusoidal voltage $U$ on the IES at $\beta_g = 35°$.

pendicular and parallel to the optical axis are $n_\perp = 1.495$ and $n_\parallel = 1.595$, respectively. The ratio of these refractive indices points to the possibility of existence of localised TM modes (the electric field vector of the wave lies in the $xz$ plane). In this case, the mode propagation parameters are determined by the refractive index of the extraordinary wave, which depends on the grazing angle as

$$n_e(\varphi) = \frac{n_\perp n_\parallel}{\sqrt{n_\parallel^2 - (n_\parallel^2 - n_\perp^2)\cos^2\varphi}}. \quad (1)$$

The TE modes (the electric field vector is directed perpendicular to the optical axis and along the $y$ axis) are not localised and leak into the cover glass plate since the refractive index of the ordinary wave $n_o \equiv n_\perp$ is in this case smaller than $n_g$.

In the geometrical optics approximation, waveguide modes are characterised by the self-consistency condition, which means that the sum of all phase shifts of a wave passed one period of its zig-zag trajectory ABCD (Fig. 6) is divisible by 2π. The self-consistency equation for TM modes has the form [16]

$$2kn_e(\varphi)d\sin\varphi - 2\varphi_q - 2\varphi_g = 2\pi s, \quad (2)$$

where $k = 2\pi/\lambda$ is the wave vector in vacuum; $2kn_e(\varphi)d\sin\varphi$ is the phase shift per two passes of the wave between the waveguide boundaries; $2\varphi_q$ and $2\varphi_g$ are the phase shifts due to the total internal reflection at the NLC layer–quartz plate and NLC layer–glass plate interfaces; and $s$ is an integer number $(0, 1, 2, \ldots)$ that determines the mode order. The boundary phase shifts are determined by the expression

$$\varphi_j = \arctan\left(\frac{n_e(\varphi)}{n_j^2}\frac{\sqrt{n_e^2(\varphi)\cos^2\varphi - n_j^2}}{\sin\varphi}\right), \quad (3)$$

where the index $j$ is q or g.

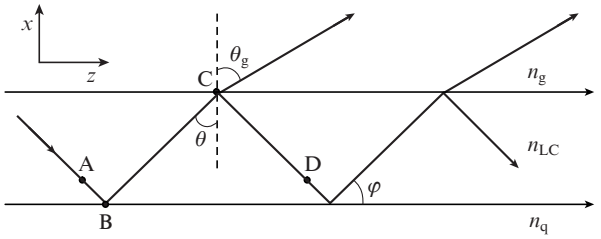


**Figure 6.** Geometrical optics of a planar dielectric waveguide with leaking modes ($\theta$, $\theta_g$ and $\varphi$ are the angles at which light beams propagate in the LC waveguide and in the glass cover plate).

From (2), we can find the dependence of the TM mode wavelength on its propagation angle,

$$\lambda_s(\varphi) = \frac{2\pi n_e(\varphi)\, d\sin\varphi}{\varphi_q + \varphi_g + \pi s}. \quad (4)$$

In the case of TE modes, the phase shift $2\varphi_g$ due to the reflection from the NLC layer–glass plate interface is equal to zero, and the self-consistency equation takes the form [16]

$$2kn_o d\sin\varphi - 2\varphi_q = 2\pi s, \quad (5)$$

where the phase shift due to the reflection from the NLC layer–quartz plate interface is determined as

$$\varphi_q = \arctan\left(\frac{\sqrt{n_o^2(\varphi)\cos^2\varphi - n_q^2}}{n_o\sin\varphi}\right). \quad (6)$$

Then, the dispersion equation, which determines the dependence of the TE mode wavelength on the propagation angle, takes the form

$$\lambda_s(\varphi) = \frac{2\pi n_o d \sin\varphi}{\varphi_q + \pi s}. \quad (7)$$

Figure 7 presents the dependences of the wavelengths of several TM and TE modes on the grazing angle in the waveguide. One can see that the radiation with a wavelength of ~600 nm can be transferred by five TM modes ($s = 0-4$) and four TE modes ($s = 0-3$). In the case of TM modes, the critical angle of incidence (total internal reflection angle) for glass is $\theta_g = 73.3°$ ($\varphi_g = 16.7°$), while this angle for quartz in the case of TE modes is $\theta_q = 77.6°$ ($\varphi_q = 12.4°$).

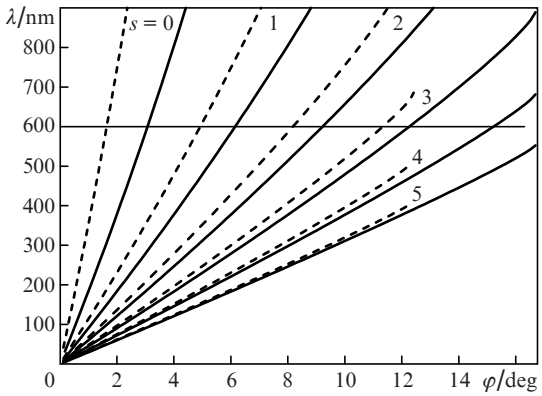


**Figure 7.** Dispersion curves of localised TM waveguide modes (solid curves) and TE modes leaking into the glass cover plate (dashed lines) for the NLC waveguide shown in Fig. 6. The horizontal line corresponds to the wavelength of interest.

### 3.2. Diffraction of a waveguide mode on the grating surface

In our case, the surface of the glass plate contacting the NLC layer had an IES, which played the role of a diffraction grating. The modes of the NLC waveguide are diffracted by the IES (Fig. 8) into beams transmitted by the glass and reflected to the waveguide layer. Let the mode $P_0-P_{0R}$ propagate in the waveguide. We denote the directions of the main maxima (diffraction orders) refracted into the glass as $P_{0T}$, $P_{-1T}$, $P_{1T}, \ldots$, $P_{-mT}$, $P_{mT}, \ldots$, and the beams reflected to the waveguide as $P_{0R}$, $P_{-1R}$, $P_{1R}$, $P_{-2R}$, $P_{2R}, \ldots$, $P_{-mR}$, $P_{mR}, \ldots$. The diffraction orders $P_{1R}$, $P_{2R}, \ldots$, $P_{mR}, \ldots$ propagating in the waveguide are not shown in the figure because they are of no interest for further consideration. The directions to the main diffraction maxima in the case of grazing incidence of a beam from a medium with a refractive index $n_{LC}$ (NLC refractive index) on a medium with a refractive index $n_g$ can be described using the vector scheme shown in Fig. 9a. From this scheme, we can write the equation for diffraction into glass as

$$\boldsymbol{k}_0 \pm m\boldsymbol{Q} = \boldsymbol{k}_{\pm m} \Rightarrow \frac{2\pi}{\lambda} n_{LC} \sin\theta \pm \frac{2\pi m}{\Lambda} = \frac{2\pi}{\lambda} n_g \sin\theta_{\pm mT}, \quad (8)$$

where

$$\theta_{\pm mT} = \arcsin\left[\frac{1}{n_g}\left(n_{LC}\sin\theta \pm m\frac{\lambda}{\Lambda}\right)\right] \quad (9)$$

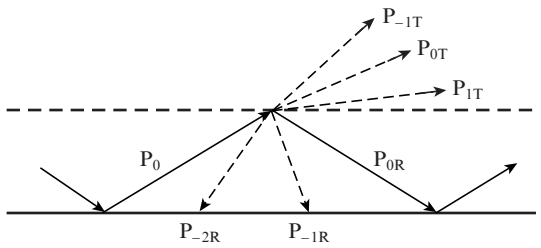


**Figure 8.** Propagation of beams in a waveguide with a diffraction grating on its upper boundary.

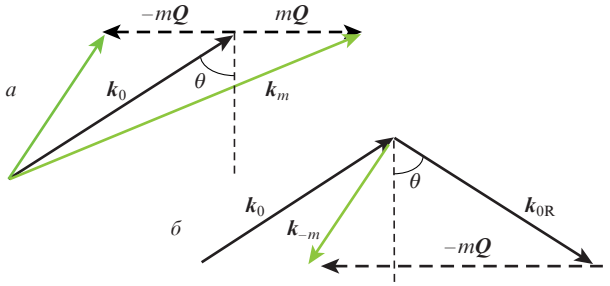


**Figure 9.** Vector schemes for calculating the directions to the main diffraction maxima into (a) glass and (b) NLC waveguide. $\boldsymbol{k}_0$ is the wave vector of the incident beam, $|\boldsymbol{Q}| = 2\pi/\Lambda$ is the modulus of the wave vector of the diffraction grating; $m$ is the diffraction order, $\boldsymbol{k}_m$ and $\boldsymbol{k}_{-m}$ are the wave vectors of beams diffracted into glass, and $\boldsymbol{k}_{0R}$ is the wave vector of the reflected beam.

are the angles of the $\pm m$-order diffraction into the glass substrate.

In the case of TM modes,

$$n_{LC} \equiv n_e(\theta) = \frac{n_\parallel n_\perp}{\sqrt{n_\parallel^2 - (n_\parallel^2 - n_\perp^2)\sin^2\theta}}$$

for a homeotropically oriented NLC layer, while for TE modes we have $n_{LC} \equiv n_o = n_\perp$.

The directions to the main diffraction maxima for reflection from the grating can be calculated using the vector scheme shown in Fig. 9b. Taking into account that we consider waveguide modes, we can write the equation for reflecting diffraction from a grating via the waveguide vectors $\beta_0$ and $\beta_{-m}$, which are the projections of the wave vector onto the waveguide axis ($z$ axis), as

$$\beta_0 - mQ = \beta_{-m} \Rightarrow \frac{2\pi}{\lambda} n_{LC}(\theta)\sin\theta - \frac{2\pi m}{\Lambda} = \frac{2\pi}{\lambda} n_{LC}(\theta_{-mR})\sin\theta_{-mR}, \quad (10)$$

where $\theta_{-mR}$ are the angles of the $-m$-order diffraction into the waveguide. For TM modes, the angles of diffraction into the NLC waveguide are determined by the formula

$$\sin\theta_{-mR} = \frac{n_\parallel[\Lambda n_e(\theta)\sin\theta - m\lambda]}{\sqrt{(n_\parallel^2 - n_\perp^2)[\Lambda n_e(\theta)\sin\theta - m\lambda]^2 + n_\parallel^2 n_\perp^2 \Lambda^2}}; \quad (11)$$

for TE modes, this formula is much simpler,

$$\sin\theta_{-mR} = \sin\theta - \frac{m\lambda}{n_o\Lambda}. \quad (12)$$

At some relation between the grating period and the mode wavelength, the $m$-order diffracted beam will be strictly opposite to the incident waveguide mode, i.e., we obtain the same feedback as in ordinary mirror cavities, which leads to lasing in the active medium. This situation is described by the formula

$$\beta_0 - mQ = \beta_{-m} = -\beta_0 \Rightarrow \frac{2\pi}{\lambda} n_{LC}(\theta)\sin\theta - \frac{2\pi m}{\Lambda}$$

$$= -\frac{2\pi}{\lambda} n_{LC}(\theta)\sin\theta, \qquad (13)$$

which can be rewritten in the form

$$2n_{LC}(\theta)\Lambda\sin\theta = m\lambda. \qquad (14)$$

In formulas (13) and (14), we omitted the subscript at the diffraction angles [see (10)]. Thus, equation (14) contains the conditions needed for the appearance of feedback at the $m$ diffraction order.

### 3.3. Estimation of lasing wavelengths and directions of their observation

To solve Eqn (14), i.e., to determine the lasing wavelength and the angle of beam propagation in the waveguide at a given diffraction grating period, let us supplement this equation with phase self-consistency equations (2) or (5). Then, to calculate the waveguide modes satisfying the oscillation condition, we obtain the system of two equations:

$$2n_{LC}(\theta)d\cos\theta = (s + \Phi/\pi)\lambda,$$

$$2n_{LC}(\theta)\Lambda\sin\theta = m\lambda, \qquad (15)$$

where $\Phi$ is the phase shift appearing due to the total internal reflection at one (TE modes) or both (TM modes) waveguide boundaries. Dividing the second equation by the first one, we obtain the following equation for calculating the propagation angle for the $s$-mode with feedback at the $m$th diffraction order:

$$\tan\theta_{s,m} = \frac{dm}{\Lambda(s + \Phi/\pi)}. \qquad (16)$$

Squaring Eqns (15) and summing them term by term, we derive the equation for the wavelength of the laser beam propagating at the angle $\theta_{s,m}$,

$$\lambda_{s,m} = \frac{2n_{LC}(\theta_{s,m})}{\sqrt{(m/\Lambda)^2 + [(s + \Phi/\pi)/d]^2}} = \frac{2n_{LC}(\theta_{s,m})d\cos\theta_{s,m}}{s + \Phi/\pi}. \qquad (17)$$

The phase shifts $\varphi_q$ and $\varphi_g$ caused by the total internal reflection from the boundaries between the LC layer and the quartz or glass plate [(3) and (6)] increase from zero at the critical angle of incidence to $\pi/2$ at grazing incidence ($\theta = \pi/2$). For numerical simulations, we ignore precise expressions for phase shifts and take an intermediate value $\Phi = \pi/4$ for all TM modes and $\pi/8$ for all TE modes. Table 1 lists the wavelengths and angles of propagation of TM and TE modes in a NLC waveguide calculated by formulas (16) and (17). As follows from Table 1, the best coincidence with the experimental data is obtained for the TM mode with $s = 4$, when feedback occurs at the 19th diffraction order, and for the TE mode with $s = 3$ at the 18th diffraction order (bolded).

**Table 1.** Oscillation wavelengths for TM and TE modes and angles of their propagation in an NLC waveguide calculated by formulas (16) and (17).

| $s$ | $m$ | $\theta_{TM}$/deg | $\lambda_{TM}$/nm | $\theta_{TE}$/deg | $\lambda_{TE}$/nm |
|---|---|---|---|---|---|
| 0 | 18 | 88.14 | 664.2 | 89.07 | 622.8 |
| | 19 | 88.23 | 629.3 | 89.12 | 590.1 |
| 1 | 18 | 84.42 | 661.4 | 85.35 | 620.9 |
| | 19 | 84.71 | 626.5 | 85.59 | 588.4 |
| 2 | 18 | 79.49 | 650.8 | 81.03 | 615.3 |
| | 19 | 81.23 | 621.1 | 82.10 | 584,5 |
| 3 | 18 | 75.93 | 640.6 | 77.43 | **608.0** |
| | 19 | 77.82 | 613.3 | 78.67 | 578.6 |
| 4 | 18 | 72.48 | 630.2 | | |
| | 19 | 73.35 | **600.2** | | |

Using formula (9), we calculated the angles of diffraction into glass for the modes that are expected to oscillate in the NLC (see Table 1) and the angles of radiation emission through the glass end face into air (observation angles). The calculation results are presented in Table 2.

**Table 2.** Angles of emission from the glass end face into air calculated by formula (9).

| $\lambda$/nm | $m$ | $\theta_g$/deg | $\varphi_g$/deg | $\beta_g$/deg |
|---|---|---|---|---|
| 608.0 TE mode | 0 | 74.86 | 16.14 | **24.97** |
| | –1 | 66.98 | 24.02 | 38.19 |
| | 1 | 79.29 | 10.71 | 16.39 |
| 600.2 TM mode | 0 | – | – | – |
| | –1 | 70.03 | 19.97 | **31.24** |
| | 1 | – | – | – |

According to Table 2, the unlocalised TE mode with $s = 3$ is diffracted into glass both in the zero and two first orders. The most intense zero order ($m = 0$) of the TE mode with $s = 3$ leaves the end face of the glass plate at the observation angle $\beta_g = 24.97°$. The localised TM mode with $s = 4$ is diffracted into glass only at $m = -1$ (we did not consider higher diffraction orders because their intensities decrease with increasing order number). This radiation leaves the glass end face at the observation angle $\beta_g = 31.24°$. Let us recall that the experimental measurements showed the peaks of TM- and TE-mode oscillation at $\beta_g = 33.1 \pm 1.5°$ and $21.8 \pm 1.8°$, respectively.

Thus, our rather rough model proposed to interpret the experimental data yields estimates of the wavelengths, polarisation and angles of observation of laser oscillation sufficiently close to the experimental values.

## 4. Conclusions

Lasing in a dye-doped NLC layer has been experimentally observed in the waveguide regime. A distributed feedback was achieved by using an IES formed on the surface of a glass cover plate that contacted the LC layer. Simultaneously, the diffraction grating in the form of a system of electrodes served for coupling out the laser radiation from the waveguide into

the glass cover plate and, through its end face, into air. The spectra of generated TM and TE waveguide modes and the angles of their observation are measured. The pump threshold for the NLC waveguide is determined. In the case of TM modes, an increase in the voltage on the IES causes a broadening of the laser line, a decrease in its intensity and a short-wavelength shift.

The simple model proposed to explain the observed experimental results predicts the possibility of feedback at the 18th diffraction order for the TE modes and at the 19th order for the TM modes of the waveguide. According to this model, the experimentally observed laser radiation is emitted from the end face of the glass substrate with an IES and corresponds to the zero-order diffraction into the glass for the TE mode and the first-order diffraction for the TM waveguide mode.

***Acknowledgements.*** The authors thank Professor L.M. Blinov for valuable comments and suggestions made when discussing the results. This work was supported by the Russian Scientific Foundation (Grant No. 13-02-12151).

## References

1. Kogelnik H., Shank C.V. *J. Appl. Phys*., **43**, 2327 (1972).
2. Vasil'eva V.V., Vinokurov D.A., Zolotarev V.V., Leshko A.Yu., Petrunov A.N., Pikhtin N.A., Rastegaeva M.G., Sokolova Z.N., Shashkin I.S., Tarasov I.S. *Fiz. Tekhn. Polupr*., **46**, 252 (2012).
3. Fricke J., Bugge F., Ginolas A., John W., Klehr A., Matalla M., Ressel P., Wenzel H., Erbert G. *IEEE Photon. Technol. Lett*., **22**, 284 (2010).
4. Fricke J., John W., Klehr A., Ressel P., Weixelbaum L., Wenzel H., Erbert G. *Semicond. Sci. Technol*., **27**, 055009 (2012).
5. Li Sh., Witjaksono G., Macomber S., Botez D. *IEEE J. Select. Topics Quantum Electron*., **9**, 1153 (2003).
6. Afonenko A.A., Aleshkin V.Ya., Dubinov A.A. *Fiz. Tekhn. Polupr*., **48**, 94 (2014).
7. Welch D.F., Parke R., Hardy A., Waarts R., Streifer W., Scifres D.R. *Electron. Lett*., **26**, 757 (1990).
8. Li Sh., Botez D. *IEEE J. Quantum Electron*., **43**, 655 (2007).
9. Il'chishin I.P., Tikhonov E.A., Tishchenko V.G., Shpak M.T. *Pis'ma Zh. Eksp. Teor. Fiz*., **32**, 27 (1980).
10. Kopp V.I., Zhang Z.-Q., Genack A. *Progr. Quantum Electron*., **27**, 369 (2003).
11. Cao W., Munos A., Palffy-Muhoray P., Taheri B. *Nature Mater*., **1**, 111 (2002).
12. Chanishvili A., Chilaya G., Petriashvili G., Barberi R., Bartolino R., Cipparrone G., Mazzulla A., Gimenes R., Oriol L., Pinol M. *Appl. Phys. Lett*., **86**, 051107 (2005).
13. Strangi G., Barna V., Caputo R., de Luca A., Versace C., Scaramuzza N., Umeton C., Bartolino R., Price G. *Phys. Rev. Lett*., **94**, 063903 (2005).
14. Palto S.P., Blinov L.M. *J. Soc. Elect. Mat. Eng*., **14**, 115 (2005).
15. Blinov L.M., Cipparrone G., Mazzulla A., Pagliusi P., Lazarev V.V., Palto S.P. *Appl. Phys. Lett*., **90**, 131103 (2007).
16. Yariv A., Yeh P. *Optical Waves in Crystals* (New York: Wiley, 1984).